Journal of Non Crystalline Solids. Vol. 351. Núm. 2. 2005. Pag. 158-166
http://dx.doi.org/10.1016/j.jnoncrysol.2004.07.069

Effect of substitution of rare earth by mischmetal on the devitrification process of Al-X-Ni-Co (X=Y, Ce, Mm) alloys.

J.S. Blázquez [1], E. Fazakas [1,2], H. Dimitrov [1], J. Latuch [1], L. Varga [2], T. Kulik [1*]

[1] *Faculty of Materials Science and Engineering, Warsaw University of Technology, Wołoska 141, 02-507 Warsaw, Poland*

[2] *Reseaerch Institute for Solid State Physics and Opptics, Hungarian Academy of Science, P.O. Box 49, Budapest 1525, Hungary*

PACS: 64.70.Kb, 61.43.Dq, 61.46.+w

Abstract

The effect of substitution of Ce or Y by mischmetal (Mm) on the glass transition and the kinetics of crystallization of quaternary Al-Ni-Co-(Ce, Y, Mm) alloys was studied using isothermal and non-isothermal calorimetry and X-ray experiments. The alloy containing Mm shows more similarity to Ce containing alloy in all the studied properties than to Y containing alloy. Glass transition is less evident for Ce and Mm containing alloys than for the alloy containing Y. For the two former alloys, the first and the second crystallization stages are strongly overlapped and yield to a fully crystallized alloy. Whereas for Y alloy, first and second stage are well resolved and the primary crystallization yields nanosized of α-Al particles embedded in a residual amorphous matrix.

Corresponding author: Prof. T. Kulik

Tel.: +48-22 660 8399

Fax: +48-22 660 8514

e-mail: tkulik@inmat.pw.edu.pl

Journal of Non Crystalline Solids. Vol. 351. Núm. 2. 2005. Pag. 158-166
http://dx.doi.org/10.1016/j.jnoncrysol.2004.07.069

1. Introduction

Amorphous Al based alloys are interesting for their excellent mechanical properties, e.g. tensile strength of the amorphous alloys is twice the highest values measured for commercial crystalline Al-based alloys [1]. Mechanical properties can be still enhanced by their partial nanocrystallization during the devitrification process [2]. The microstructure of these alloys consists of nanosized crystals of α-Al phase embedded in a residual amorphous matrix. Amorphous metallic alloys can be easily obtained by melt-spinning technique in quaternary systems containing Al, rare earth metal (RE) and two transition metals (TM) [3].

It has been found that alloys with high glass forming ability (low critical cooling rate for glass formation) are so called strong metallic glasses in the Angell plot [4]. Therefore, the study of the glass transition kinetics can give us complementary information about the glass forming ability of the amorphous alloys. On the other hand, the thermal stability of these alloys (in amorphous or nanocrystalline state) marks a limit of their applicability, therefore, the study of the kinetics of crystallization of Al-based alloys is an important task to which several studies have been devoted (for a review see [5])

Mischmetal (Mm) is a natural mixture of rare earth metals, normally Ce, La and Nd. This mixture, due to the similar properties of its constituent, requires complex procedures to separate them. Replacement of pure RE by Mm reduces several times the cost of the material. Because Mm can exhibit different concentration of elements depending on several factors (place of extraction, for example), it is important to compare the behavior of Mm substituted alloys with those with pure rare earth elements [5-7].

In this study the devitrification process and the kinetics of crystallization was studied on three different alloys of nominal compositions $Al_{85}X_8Ni_5Co_2$, with X = Mm, Ce and Y (from the point of view of this study, Y is considered as a RE element). Ce is the main component of the Mm used in this study. On the other hand, $Al_{85}Y_8Ni_5Co_2$ exhibits one of the

Journal of Non Crystalline Solids. Vol. 351. Núm. 2. 2005. Pag. 158-166
http://dx.doi.org/10.1016/j.jnoncrysol.2004.07.069

largest supercooled liquid region in Al-based alloys. The aim of this study is to assess the similarities and differences for using Mm instead of pure Ce or Y, because of Mm is several times cheaper than the pure rare earth metals.

2. Experimental

Amorphous ribbons of $Al_{85}X_8Ni_5Co_2$ (X = Mm, Ce, Y), were obtained by melt spinning technique. For convenience, in this work the Mm, Ce and Y containing alloys are named Mm alloy, Ce alloy and Y alloy, respectively. Composition of the mischmetal used in this work is following: Ce-50.3 at. %, La-43.5 at. %, Pr-5.9 at. % and Nd-0.3 at. %. Differential scanning calorimetry (DSC) experiments were performed on a Perkin-Elmer DSC7 calorimeter. Microstructure was studied by X-ray diffraction (XRD) using Co-K_α radiation

3. Devitrification process

3.1 DSC.

Figure 1 shows DSC scans for the three alloys studied at the heating rate of 10 K/min. The glass transition can be observed for each alloy as an endothermic process occurring before the crystallization onset, as it is shown in Figure 2. In this figure, DSC scans at the scanning rate of 80 K/min are presented. Definition of glass transition temperature, T_g, is somehow ambiguous. In this work, it was defined as the intersection of the steepest slope with the baseline at low temperature, which might be the glass transition onset [8]. These values are indicated by arrows in Fig. 2. However, other authors [9] define T_g as the inflexion point of the endothermic effect. In the latter definition T_g values are higher and, consequently, supercooled liquid region decreases (in our case by about 10 K).

Journal of Non Crystalline Solids. Vol. 351. Núm. 2. 2005. Pag. 158-166
http://dx.doi.org/10.1016/j.jnoncrysol.2004.07.069

T_g decreases in the order Mm>Ce>Y and supercooled liquid range, calculated as the difference between T_g and crystallization onset temperature, T_x, decreases in the opposite order, Y>Ce>Mm, being similar for the Ce and Mm alloys (~ 20 K) and clearly larger in the Y alloy (~ 30 K). The magnitude of the endothermic effect follows the same trend as the width of the supercooled liquid range. The dependence of the glass transition temperature on heating rate was evaluated in the frame of Vogel-Fulcher-Tammann (VFT) equation [8]:

$$\beta(T_g)=B\ exp[DT_g^0/(T_g^0-T_g)] \qquad (1)$$

where β is the scanning rate, T_g is the glass transition temperature, B is a constant, D is the strength parameter and T_g^0 is the asymptotic value of T_g. To fit the experimental data, logarithm was taken on equation 1:

$$Ln\beta(T_g)=LnB+DT_g^0/(T_g^0-T_g) \qquad (2)$$

In our case, T_g^0 was estimated to be about 175 K below the glass transition temperature, T_g, assuming a linear relation between $Ln\beta$ and $1/(T_g^0-T_g)$, as VFT equation predicts. This difference between T_g and T_g^0, ΔT_g^0, is much larger than those found for other metallic glasses as $Pd_{40}Ni_{40}P_{19}Si_1$ and $Pd_{77.5}Si_{16.5}Ag_6$ ($\Delta T_g^0 \approx 60$ K) [8], but of the same order as in $La_{55}Al_{25}Ni_{20}$ [8], $(FeCoBC)_{80}Si_3Al_5Ga_2P_{10}$ [10] and $(CoFe)_{62}Nb_6Zr_2B_{30}$ [11]. From the slope of this representation, D was estimated. Other parameter which can be obtained from the analysis of the glass transition parameters is the fragility, m, calculated from:

$$m=(DT_g^0T_g)/[(T_g-T_g^0)^2Ln10] \qquad (3)$$

The results of this analysis are summarized in Table I. The parameter that shows more confidence is D, for which values of similar order of magnitude were found for $(CoFe)_{62}Nb_6Zr_2B_{30}$ [11] but smaller for $(FeCoBC)_{80}Si_3Al_5Ga_2P_{10}$ [10]. In spite of the uncertainty of the value of m, derived from the high error of the estimation of T_g^0, a value of 30 for the fragility indicates that the studied amorphous systems lie between the strong and

Journal of Non Crystalline Solids. Vol. 351. Núm. 2. 2005. Pag. 158-166
http://dx.doi.org/10.1016/j.jnoncrysol.2004.07.069

fragile extremes of Angell's classification [4] and suggests a good glass-forming ability for these alloys, as it has been observed for similar compositions [5].

Most relevant parameters of crystallization process, calculated from DSC plots obtained at a scanning rate of 10 K/min, are summarized in Table II. The thermal stability of the amorphous state increases in the order Y<Ce<Mm. In Ce alloy, only two stages are detected during the crystallization process, although at higher heating rates the first peak becomes broader and a "two-peak" structure is observed. Three stages are clearly resolved in Y alloy and, for the case of Mm, three stages can be also observed but with a very important overlapping between the two former stages. The crystallization temperature range can be defined as the difference between the end of the last exothermic peak and the onset temperature. In Ce alloy crystallization process occurs in a smaller temperature range (about 30 K at 10 K/min) than in the other two alloys. The crystallization temperature range increases up to 45 K in Mm alloy. However the widest range was found in Y alloy, more than 100 K, for which the first and the second transformation stages are well resolved.

The relative enthalpy, calculated as the ratio between the enthalpy of the transformation stage and the total enthalpy of the crystallization process, give us information about the relative weight of every transformation stage. In the case of the first crystallization stage of Ce alloy, this parameter is 60 %, similar to that of the first plus second stages in Mm alloy, 68 %. However, for Y alloy, the relative enthalpy of the first stage is clearly lower, 32 %, although adding the second stage a value close to those of the other alloys is obtained, 64 %.

3.2 XRD.

Journal of Non Crystalline Solids. Vol. 351. Núm. 2. 2005. Pag. 158-166
http://dx.doi.org/10.1016/j.jnoncrysol.2004.07.069

Figures 3 to 5 show the XRD patterns obtained from samples of the different alloys annealed up to the end of the different stages of crystallization at 10 K/min. Amorphous patterns obtained for the as-cast ribbons are also shown.

In the case of Mm alloy, to have some information about the first process, a sample was annealed below the peak temperature of this stage. No difference in number and positions of the X-ray peaks was found between this sample and that annealed behind the second transformation stage, which might be due to the high overlapping between these two stages. Although some peaks were identified to belong to fcc α-Al, orthorhombic $Al_{11}Mm_3$ or orthorhombic Al_3Ni phases, most of them were unidentified. XRD pattern changes drastically after annealing behind the third crystallization event. Most of the peaks correspond to $Al_{11}Mm_3$ phase, but peaks corresponding to fcc α-Al and orthorhombic Al_3Ni phases also increase their intensity, whereas those peaks assigned to the unidentified phase(s) disappear, indicating a metastable character for the phase(s).

Ce alloy exhibits very similar crystallization products to those of the Mm alloy and no remarkable differences can be found between the XRD patterns obtained for samples annealed at equivalent stages of crystallization.

On the other hand, Y alloy shows very different crystallization processes. After the first crystallization stage, fcc α-Al appears as the main phase together with an important amorphous halo. Small traces of an unidentified phase can also be detected. Neglecting the presence of these traces, crystalline volume fraction can be estimated from the ratio between the areas of the crystalline (111) peak and the amorphous halo. A deconvolution process was performed to measure the areas. Crystalline contribution was fitted using a Lorentzian function, which is expected to describe the small grain size effects. Amorphous contribution was fitted using a Gaussian contribution. The percentage of crystalline contribution to the total intensity was calculated to be 21 %. The very different composition of the crystalline

Journal of Non Crystalline Solids. Vol. 351. Núm. 2. 2005. Pag. 158-166
http://dx.doi.org/10.1016/j.jnoncrysol.2004.07.069

(close to pure Al, which is a light atom, due to the very low solubility of the other elements in fcc α-Al) and amorphous phase (enriched in Y, Ni and Co much heavier than Al) makes it necessary to take into account the different average scattering power of every phase. This correction was explained elsewhere for Fe based alloys [12]. The corrected value gives us a larger value of crystalline volume fraction after the first crystallization, 27 %. Size of α-Al crystals after the first crystallization event was calculated from Scherrer formula to be 13 nm. Therefore, annealing behind the first peak in Y alloy results in nanocrystalline microstructure formation, unlike for Ce and Mm alloys.

For samples annealed above the second crystallization stage of Y alloy, intensity of α-Al peaks increases and they become narrower indicating an increase of the grain size of this phase. On the other hand, diffraction maxima of unidentified phase(s) appear. After the third crystallization event, peaks of this unidentified phase(s) are reduced and hexagonal Al_3Y and orthorhombic Al_3Ni are detected. fcc α-Al remains the most important phase, with narrower peaks than in the previous stages, indicating that grain growth of this phase also occurs during the third stage.

The importance of α-Al phase in Y alloy contrasts with the low intensity assigned to this phase in Mm and Ce alloys, for which crystallization products are very similar. The rare earth compound in the case of these alloys is richer in Al than in Y alloy (~ 80 and 75 %, respectively). Although this difference could explain qualitatively a larger amount of fcc α-Al in Y alloy, the magnitude of the difference is too large to be explained only in this way. Another effect can be found in the binary alloys of Al-RE systems [5]. In Al-Y system the supersaturated solution of Y in fcc α-Al obtained by rapid quenching extends up to 9 at % of Y, whereas in Al-Ce and Al-La (Ce and La are the main ingredients in the Mm used in this study) is only 7 at % [5]. Although these values are valid only for binary alloys obtained after rapid quenching from the melt, they give us an idea of the solubility of each rare earth

Journal of Non Crystalline Solids. Vol. 351. Núm. 2. 2005. Pag. 158-166
http://dx.doi.org/10.1016/j.jnoncrysol.2004.07.069

element on α-Al phase. The lower solubility of Ce and La compared to Y in fcc α-Al phase makes the formation of this phase in Ce and Mm alloy more difficult than in Y alloy.

4. Crystallization kinetics.

4.1 Non-isothermal crystallization kinetics.

Non isothermal kinetics of crystallization was studied using Kissinger [13] and Augis-Bennett [14] approximations. Kissinger approximation is widely used to obtain activation energies, E_a, of the crystallization of metallic glasses. However, the theoretical fundament of this method is hardly extended to the crystallization of metallic amorphous [14]. This method needs only the values of the peak temperature, T_P, (assumed to be the temperature at which the transformation rate is maximum) for different heating rates. E_a is obtained from the slope of the plot of $Ln(\beta/T_P^2)$ versus $1/T_P$ [13].

In Augis-Bennett method, onset crystallization temperature, T_x, is needed. E_a is obtained from the slope of $Ln[\beta/(T_P-T_x)]$ versus $1/T_P$ [14]. This method requires more information than that of Kissinger, for which the shape of the DSC peak has no effect, unlike Augis-Bennett (the distance between T_x and T_P is considered). Due to the overlapping between the first and the second crystallization stage, Augis-Bennett method was not applied to the second transformation stage.

Linear fittings are shown in figure 6 for the first and the second transformation stages and in figure 7 for the third (second in the case of Ce) transformation stage. The results are summarized in Table III. As it can be seen, good agreement can be found in all compared cases between Kissinger and Augis Bennett method, except for those of the first peak in Ce and Mm alloy. The best linear fitting for this peak was obtained from Kissinger plots (see figure 1). This could be due to the large overlapping between the first and the second crystallization stages in Mm alloy which seems to be even larger in the case of Ce, for which

Journal of Non Crystalline Solids. Vol. 351. Núm. 2. 2005. Pag. 158-166
http://dx.doi.org/10.1016/j.jnoncrysol.2004.07.069

only one event is detected during heating at 10 K/min (see figure 1). This overlapping must affect the calculated value for the onset temperature used in Augis-Bennett approximation. In the case of Kissinger an average value is obtained.

In the case of the first crystallization peak (and taking into consideration the values obtained from Kissinger approximation), very similar values of E_a were observed for the three studied composition. Although the crystallization products after the first transformation stage are so different between Y and the other two alloys, activation energy for Y alloy is only slightly lower than in the case of Ce and Mm alloys (2.5 eV and 2.8-2.9 eV, respectively). Similar values of E_a have been observed in $Al_{85}(NiY)_{15}$ series for the primary crystallization (~ 3 eV) [15], although lower values were found for the primary crystallization of Al-based alloys with low RE content, 3 at. % (~ 1.5 eV) [16]. At the last crystallization stage (which yields to the stable phases $Al_{11}Mm_3$, $Al_{11}Ce_3$ and Al_3Y for Mm, Ce and Y, respectively) E_a is very similar in all the studied cases (~ 1.7 eV).

4.2 Isothermal crystallization kinetics.

Aiming at having a deeper knowledge of the crystallization kinetics of the studied alloys, isothermal DSC experiments were performed at three different temperatures for 2 h. Annealing temperature, T_a, was reached in two steps: first, the sample was heated at 200 K/min up to 20 K below the desired temperature and then it was heated up to the desired temperature at 10 K/min. With this procedure we tried to avoid annealing previous to the real isotherm and to minimize the effect of the transitory.

Figure 8 shows isothermal scans for the three alloys studied. Two exothermic peaks are clearly observed in the case of Ce and Mm alloys, however, only one event is detected in the case of Y. To have additional information, after isothermal treatment, the samples were submitted to a continuous heating at 40 K/min. This enables us to compare the enthalpy

Journal of Non Crystalline Solids. Vol. 351. Núm. 2. 2005. Pag. 158-166
http://dx.doi.org/10.1016/j.jnoncrysol.2004.07.069

values and to do a correspondence between isothermal and non-isothermal stages. Table IV presents the enthalpy values for the different peaks observed in isothermal scans as well as the residual enthalpy measured in non-isothermal scans performed on the samples after isothermal annealing.

As it is seen in figure 9, in the case of Ce and Mm alloys, after annealing, only one small residual peak is observed during continuous heating. However, for Y alloy, two overlapped peaks are detected. Whereas in the case of Ce, the small residual peak shows no difference with the annealing temperature, for Mm alloy the sample annealed at the lowest temperature for 2 h shows an increase of the enthalpy of the residual DSC peak during continuous heating. This is in agreement with the observed uncompleted second isothermal transformation stage for this alloy at this temperature after annealing for 2 h. The enthalpy values of the first isothermal event reflects that this event corresponds to the first stage in the case of Ce alloy and to the first and second stage in the case of Mm. The second isothermal stage might correspond to the second and third non isothermal events in the case of Ce and Mm alloy respectively, which exhibits similar enthalpy values. In the case of Mm alloy, the separation in time between the two processes is larger, in agreement with the larger separation in temperature between the first and the third process for continuous heating in Mm alloy compared to Ce alloy (see for example Fig. 1 or Table II). Negligible annealing temperature dependence was found for the peak temperature of the residual process detected during continuous heating after isothermal annealing (for samples at which the second isothermal event was completed).

In the case of Y alloy, the continuous evolution of the residual DSC peaks with the annealing temperature indicates that the isothermal process is extended over a larger time range than 2 h and, as in the cases of Mm and Ce alloys, the first event corresponds not only to the first non-isothermal crystallization stage but also affects the second one. The enthalpy

Journal of Non Crystalline Solids. Vol. 351. Núm. 2. 2005. Pag. 158-166
http://dx.doi.org/10.1016/j.jnoncrysol.2004.07.069

involved in the first isothermal DSC peak is nearly constant. Therefore, a very broad tail or second peak which is too broad to be detected in isothermal scanning might be invoked to describe the effects observed during the continuous scans performed after the isothermal annealing. In non-isothermal scans after isothermal annealing, two main peaks are detected. The enthalpy of the first one strongly decreases as T_a increases, with no changes of the peak temperature. Enthalpy of the second peak also decreases slightly, and the peak temperature shifts to lower values. At temperatures higher than the second event detected from non-isothermal scanning after isothermal treatments, smaller exothermic peaks can be observed.

Isothermal kinetics of crystallization was studied in the frame of Johnson-Mehl-Avrami theory (JMA) [17]. JMA theory gives the transformed fraction, x, versus the annealing time as:

$$x = exp\{-[K(t-t_0)]^n\} \qquad (4)$$

where K is the frequency factor, t is the time, t_0 is the incubation time for the process and n is the Avrami exponent. Avrami exponent can be easily obtained as the slope of $Ln(-Ln(1-x))$ versus $Ln(t-t_0)$, JMA plot.

Figure 10 shows JMA plots for samples with different fraction of transformed phase ($0.2 < x < 0.8$) for the first isothermal peak. Figure 11 shows JMA plots for the same interval of transformed fraction corresponding to the second isothermal event detected in Ce and Mm alloys. Linear regime in JMA plots is better fulfilled for the second peak. For the first isothermal peak overlapping between the signal due to the transformation process and the transitory from the change of heating to isothermal conditions in the DSC, affects the processes with low incubation time at low transformed fractions. However, in the case of Y alloy, a clear deviation from linearity is observed. JMA plot of Y alloy samples can be divided in two steps as it was also found for the nanocrystallization process of other Al-RE-TM [18], Fe-based [19] and FeCo-based alloys [20]. The second step corresponds to a slow

Journal of Non Crystalline Solids. Vol. 351. Núm. 2. 2005. Pag. 158-166
http://dx.doi.org/10.1016/j.jnoncrysol.2004.07.069

down in the kinetics of nanocrystallization, which can be related to the end of nucleation of α-Al phase and consequently to the growth of the nanocrystals, strongly hindered by Y atoms, with slow diffusivity and low solubility in the α-Al phase.

Activation energy of the different processes can be obtained from the evolution of the incubation time with the temperature. Table V shows E_a values obtained from this procedure along with the n values for the different studied alloys. The lowest Avrami exponent corresponds to Y alloy, which in the second step of the JMA plot exhibits values below 1. Low values, about 1, were previously reported for nanocrystallization of Al-based alloys [16]. The first isothermal event shows values of the Avrami exponent between 1.5 and 1.9, lower than that observed for the second isothermal peak with n = 2.3-2.5. A value of n = 2.5 could be assigned to constant nucleation and 3 dimensional diffusion controlled growth, lower values could be explained by a decreasing nucleation along the transformation ($1.5 < n < 2.5$) or even no nucleation (n = 1.5) [21], because of the existence of frozen prenuclei in the melt-spun ribbons. These values are smaller than those found for $Al_{85}(YNd)_8Ni_5Co_2$ (n = 2.7-5) [22].

Values of E_a obtained with isothermal methods are clearly higher than those obtained using non-isothermal methods (see Table III). In fact, the values of E_a calculated with different methods correspond to different processes. In the case of the value obtained from incubation time of isothermal events, E_a corresponds to the activation energy at 0 % of transformed fraction. On the other hand, Kissinger's value corresponds to the peak temperature on non-isothermal annealing, which in our case appears for about 50 % of the total transformation. Values of E_a obtained from isothermal analysis of crystallization of amorphous alloys of similar compositions are 2.8-4 eV, similar to those found in this study [18,22]

Journal of Non Crystalline Solids. Vol. 351. Núm. 2. 2005. Pag. 158-166
http://dx.doi.org/10.1016/j.jnoncrysol.2004.07.069

It is possible to calculate a local activation energy, $E_a(x)$, [23] versus the transformed fraction, assuming an Arrhenius dependence for the time necessary to reach a selected x with the annealing temperature, T_a.

$$t(x) = \tau exp[E_a(x)/RT_a] \qquad (5)$$

where τ is a constant.

Figure 12 shows the plot of activation energy versus x for different samples and different isothermal events detected. $E_a(x)$ is almost constant for Mm and Ce alloys for the first and the second crystallization stage, and higher than the corresponding E_a obtained from Kissinger's method. However, in the case of Y alloy, $E_a(x)$ continuously decreases down to $x = 0.8$ and the values are in agreement with the corresponding ones obtained from Kissinger's method in the range of x: $0.2 < x < 0.5$. The disagreement observed for the other cases can be due to the complexity of the crystallization processes, for which not only one phase, but even metastable phase(s) are formed, the formation of which might depend on the annealing conditions. In the case of Y alloy, other phases, except residual amorphous and α-Al, can be neglected after the first crystallization stage.

5 Conclusions.

The behavior of the alloy containing Mm is similar to that of the alloy containing pure Ce for all the studied properties and some differences arise between these two alloys and the alloy with Y.

- Glass transition temperature decreases in the order Y > Ce > Mm, being in the Y alloy enhanced with respect to the other two alloys.
- From Vogel-Fulcher-Tammann analysis, intermediate situation between fragile and strong amorphous alloys and good glass forming ability is suggested for all the alloys studied.

Journal of Non Crystalline Solids. Vol. 351. Núm. 2. 2005. Pag. 158-166
http://dx.doi.org/10.1016/j.jnoncrysol.2004.07.069

- Thermal stability of amorphous phase increases in the order Y < Ce < Mm.
- The alloy with Y is the only one of the studied series in which a nanocrystalline structure is developed during devitrification process.
- Devitrification process in Mm and Ce alloys can be summarized as follows:

Amorphous→α-Al + metastable unidentified phase(s)→ α-Al + $Al_3Ni(Co)$ + $Al_{11}Ce(Mm)_3$

and in the case of Y alloy

Amorphous→α-Al + residual amorphous→α-Al + metastable unidentified phase(s)→

→α-Al + $Al_3Ni(Co)$ + Al_3Y

- Slower crystallization kinetics was found in Y alloy, for which *n*, at low values of transformed fraction, is 1.5, decreasing at high transformed fraction to 0.5.

Acknowledgement

This work was supported by EU Research Training Network (Contract Number HPRN-CT-2000-00038).

Journal of Non Crystalline Solids. Vol. 351. Núm. 2. 2005. Pag. 158-166
http://dx.doi.org/10.1016/j.jnoncrysol.2004.07.069

References

[1] A. Inoue, K. Ohtera, A.P. Tsai, T. Masumoto, J. Jpn. Appl. Phys. 27 (1998) L280.

[2] Y.H. Kim, A. Inoue, T. Masumoto, Mater. Trans. JIM 31 (1990) 747.

[3] J. Latuch, H. Matyja, V.I. Fadeeva, Mat. Sci. Eng. A179-180 (1994) 506.

[4] C.A. Angell, Science 267 (1995) 1924.

[5] Inoue, Prog. Mater. Sci. 43 (1998) 365.

[6] D.V. Louzguine, A.R. Yavari, A. Inoue, J. Non-Crystal. Solids 316 (2003) 255.

[7] I.T.H. Chang, R.R. Botten, Mat. Sci. Eng. A226-228 (1997) 183.

[8] R. Brunning, K. Samwer, Phys. Rev. B 46 (1992) 11318.

[9] Users Manual 1020 Series DSC7 Thermal Analysis System, The Perkin-Elmer Corporation, 1993, p. 5-38.

[10] J.M. Borrego, C.F. Conde, A. Conde, S. Roth, H. Grahl, A. Ostwald, J. Eckert, J. Appl. Phys. 92 (2002) 6607.

[11] J.M. Borrego, A. Conde, S. Roth, J. Eckert, J. Appl. Phys. 92 (2002) 2073.

[12] J.S. Blazquez, V. Franco, C.F. Conde, A. Conde, J. Magn. Magn. Mat. 254-255 (2003) 460.

[13] H.E. Kissinger, Anal. Chem. 29 (1957) 1702.

[14] J.A. Augis, J.E. Bennett, J. Therm. Anal. 13 (1978) 283.

[15] S. Saini, A. Zaluska, Z. Altounian, J. Non-Crystal. Solids 250-252 (1999) 714.

[16] A.P. Tsai, T. Kamiyama, Y. Kawamura, A. Inoue, T. Masumoto, Acta Mater. 45 (1997) 1477.

[17] M. Avrami, J. Chem. Phys. 9 (1991) 177.

[18] A.K. Gangopadhyay, T.K. Croat, K.F. Kelton, Acta Mater. 48 (2000) 4035.

[19] K. Suzuki, J.M. Cadogan, J.B. Dunlop, V. Sahajwalla, Appl. Phys. Letters 67 (1995) 1369.

Journal of Non Crystalline Solids. Vol. 351. Núm. 2. 2005. Pag. 158-166
http://dx.doi.org/10.1016/j.jnoncrysol.2004.07.069

[20] J.S. Blazquez, C.F. Conde, A. Conde, Appl. Phys. A 76 (2003) 575.

[21] J.W. Christian, in: Theory of Transformations in Metals and Alloys, Part I, Pergamon, Oxford, 1975, p. 542.

[22] D.V. Louzguine, A. Inoue, J. Non-Crystal. Solids 311 (2002) 281.

[23] K. Lu, J.T. Wang, Mater. Sci. Eng. A133 (1991) 500.

Journal of Non Crystalline Solids. Vol. 351. Núm. 2. 2005. Pag. 158-166
http://dx.doi.org/10.1016/j.jnoncrysol.2004.07.069

Figure Captions

Figure 1: DSC scans at 10 K/min for as-cast samples of the three alloys studied.

Figure 2: DSC scans at 80 K/min for as-cast samples of the three alloys studied in the glass transition region. The arrows indicate the glass transition temperature estimated as the intersection of the steepest slope with the baseline at low temperatures.

Figure 3: XRD patterns for samples of Mm alloy heated up to different temperatures at 10 K/min.

Figure 4: XRD patterns for samples of Ce alloy heated up to different temperatures at 10 K/min.

Figure 5: XRD patterns for samples of Y alloy heated up to different temperatures at 10 K/min.

Figure 6: Kissinger's and Augis-Bennett's plots for the first, in the case of Ce alloy, and first and second, in the case of Mm and Y alloys, crystallization stages detected using DSC.

Figure 7: Kissinger's and Augis-Bennett's plots for the second, in the case of Ce alloy, and third, in the case of Mm and Y alloys, crystallization stages detected using DSC.

Figure 8: Isothermal DSC plots recorded during annealing at different temperatures for 2 h of the three alloys studied.

Figure 9: DSC scans at 40 K/min for the samples preannealed at different temperatures for 2h.

Figure 10: JMA plots for the first peak recorded during isothermal annealing at three different temperatures for the three alloys studied.

Figure 11: JMA plots for the second peak recorded during isothermal annealing at three different temperatures for Ce and Mm alloys.

Figure 12: Local values of the activation energy calculated from the isothermal annealing data for the three alloys studied.

Journal of Non Crystalline Solids. Vol. 351. Núm. 2. 2005. Pag. 158-166
http://dx.doi.org/10.1016/j.jnoncrysol.2004.07.069

Table I

Glass transition parameters for the three alloys studied by DSC. Supercooled liquid range (ΔT_x) obtained at 80 K/min, asymptotic value of glass transition temperature (T_g^0), strength (D) and fragility (m).

$Al_{85}X_8Ni_5Co_2$	ΔT_x (± 2 K)	T_g^0 (± 50 K)	D	m ± 30
Mm	17	400	8 ± 2	30
Ce	19	400	9 ± 2	30
Y	29	375	10 ± 3	30

Journal of Non Crystalline Solids. Vol. 351. Núm. 2. 2005. Pag. 158-166
http://dx.doi.org/10.1016/j.jnoncrysol.2004.07.069

Table II

Crystallization parameters for the three alloys studied obtained by DSC. Crystallization onset temperature (T_x), peak temperatures (T_P) and enthalpy (H), of the different crystallization stages.

$Al_{85}X_8Ni_5Co_2$	T_x (± 1 K)	T_{P1} (± 0.5 K)	T_{P2} (± 0.5 K)	T_{P3} (± 0.5 K)	H_1 (± 5 J/g)	H_2 (± 5 J/g)	H_3 (± 5 J/g)
Mm	575	579	583	611	74		51
Ce	570	572		592	86		41
Y	557	561	603	656	48	47	53

Journal of Non Crystalline Solids. Vol. 351. Núm. 2. 2005. Pag. 158-166
http://dx.doi.org/10.1016/j.jnoncrysol.2004.07.069

Table III

Kinetic parameters of the crystallization process of the three alloys studied by non-iosthermal DSC analysis.

$Al_{85}X_8Ni_5Co_2$		E_a Kissinger (± 0.5 eV)	E_a Augis-Bennett (± 0.5 eV)
Mm	1st peak	2.9	2.1
	2nd peak	2.3	--
	3rd peak	1.7	1.6
Ce	1st peak	2.8	1.3
	2nd peak	1.5	1.9
Y	1st peak	2.5	2.1
	2nd peak	2.7	--
	3rd peak	1.7	2.0

Journal of Non Crystalline Solids. Vol. 351. Núm. 2. 2005. Pag. 158-166
http://dx.doi.org/10.1016/j.jnoncrysol.2004.07.069

Table IV

Enthalpy values (*H*) of the as-quenched alloys studied isothermally at temperatures T_a and the same alloys, after preannealing, during continuous heating at 40 K/min.

$Al_{85}X_8Ni_5Co_2$	T_a (K)	Isotherm		Non-isotherm	
		H_1 (± 10 J/g)	H_2 (± 5 J/g)	H (± 5 J/g)	
Mm	568	90	47	16	
	563	93	53	16	
	558	85	--	35	
Ce	563	91	60	16	
	558	89	53	17	
	553	87	54	18	
Y	548	81		6	32
	543	87		24	36
	538	82		37	43

Journal of Non Crystalline Solids. Vol. 351. Núm. 2. 2005. Pag. 158-166
http://dx.doi.org/10.1016/j.jnoncrysol.2004.07.069

Table V

Kinetic parameters of the crystallization process of the three alloys studied by isothermal DSC analysis.

$Al_{85}X_8Ni_5Co_2$		E_a (eV)	n (± 0.5)
Mm	1st peak	3.8 ± 0.1	1.6
	2nd peak	3.8 ± 0.6	2.5
Ce	1st peak	4.2 ± 0.9	1.9
	2nd peak	4.5 ± 1.4	2.3
Y	1st peak	4.7 ± 0.3	1.5
			0.5

Journal of Non Crystalline Solids. Vol. 351. Núm. 2. 2005. Pag. 158-166
http://dx.doi.org/10.1016/j.jnoncrysol.2004.07.069

Figure 1

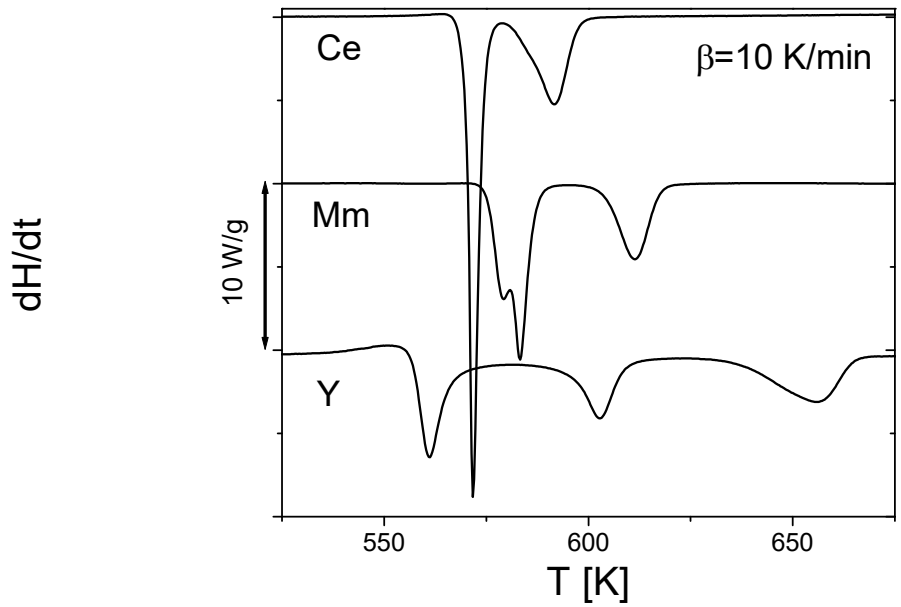

Figure 2

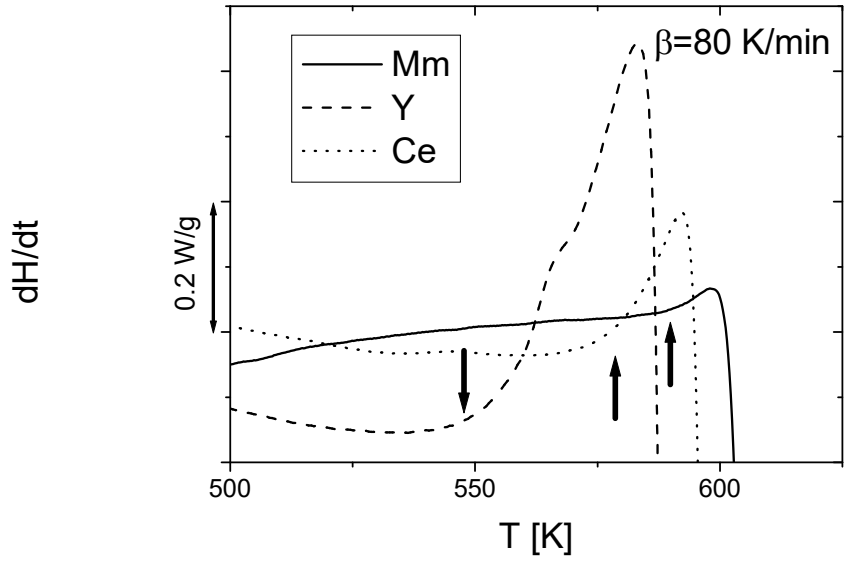

Journal of Non Crystalline Solids. Vol. 351. Núm. 2. 2005. Pag. 158-166
http://dx.doi.org/10.1016/j.jnoncrysol.2004.07.069

Figure 3

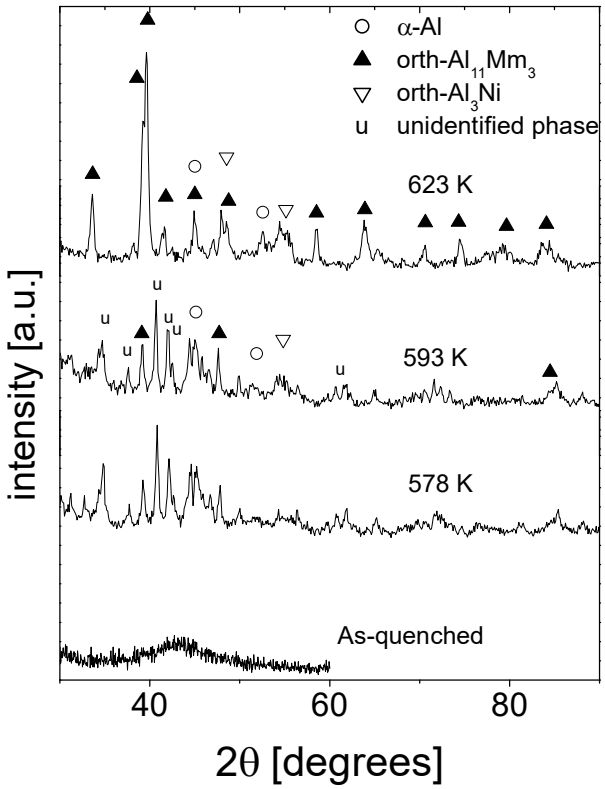

Journal of Non Crystalline Solids. Vol. 351. Núm. 2. 2005. Pag. 158-166
http://dx.doi.org/10.1016/j.jnoncrysol.2004.07.069

Figure 4

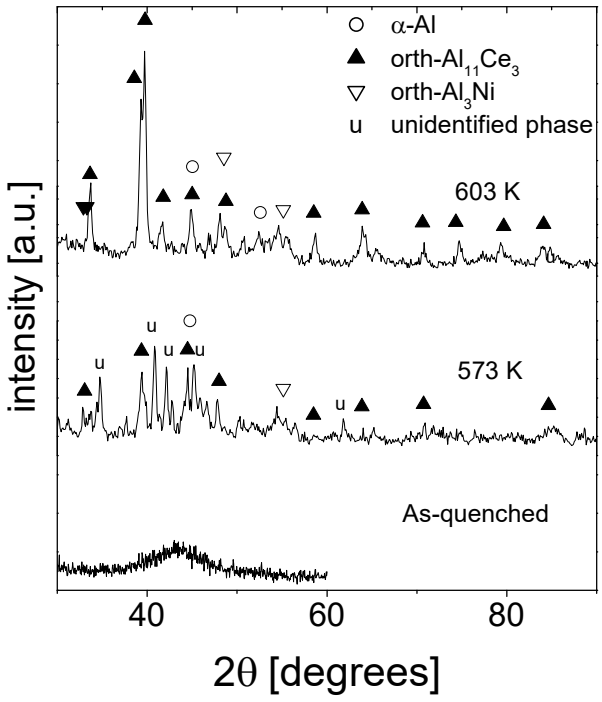

Journal of Non Crystalline Solids. Vol. 351. Núm. 2. 2005. Pag. 158-166
http://dx.doi.org/10.1016/j.jnoncrysol.2004.07.069

Figure 5

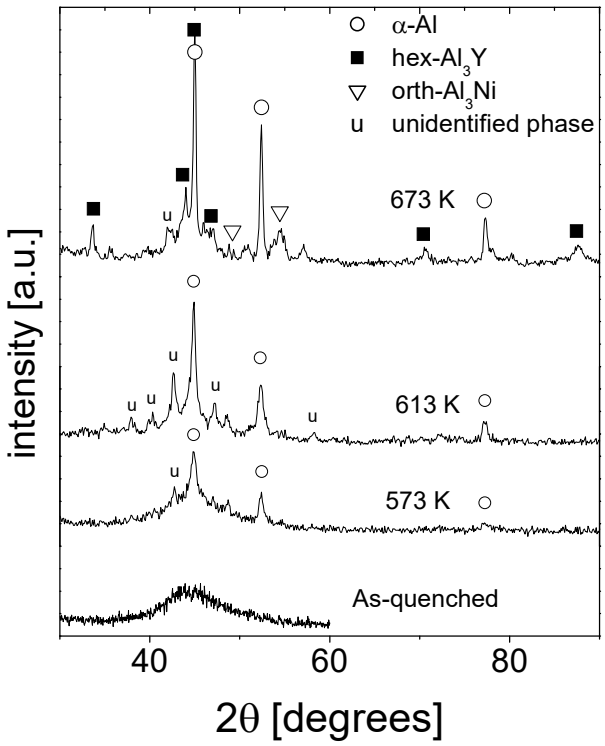

Figure 6

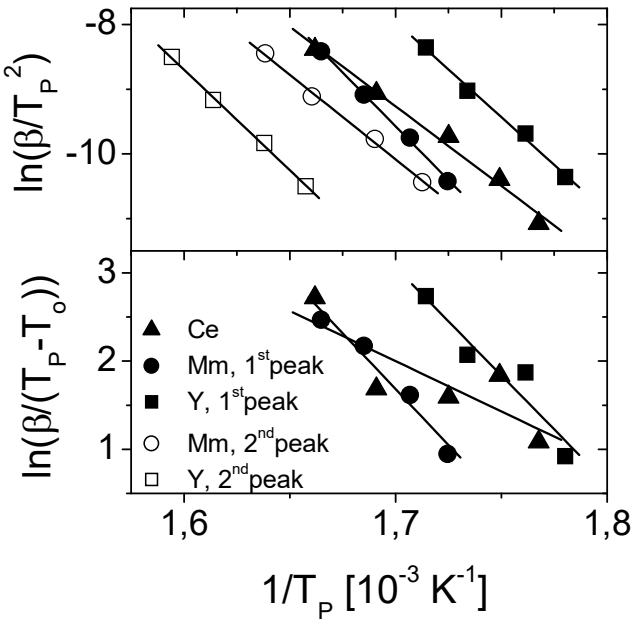

Journal of Non Crystalline Solids. Vol. 351. Núm. 2. 2005. Pag. 158-166
http://dx.doi.org/10.1016/j.jnoncrysol.2004.07.069

Figure 7

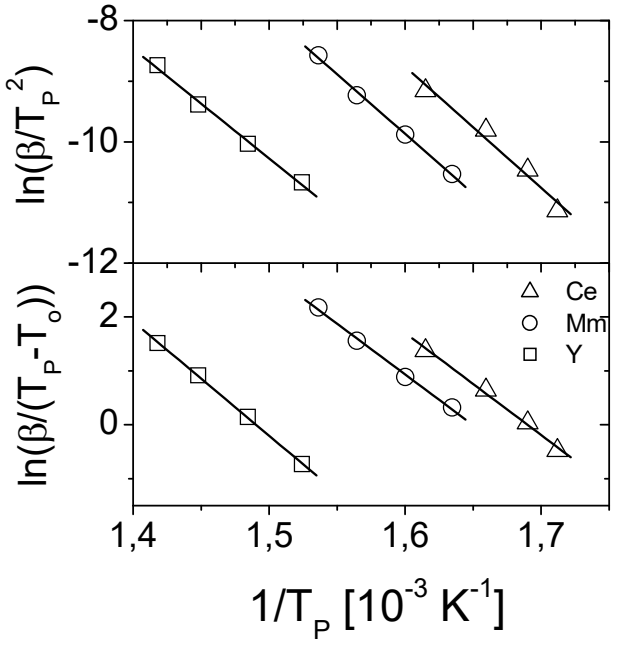

Journal of Non Crystalline Solids. Vol. 351. Núm. 2. 2005. Pag. 158-166
http://dx.doi.org/10.1016/j.jnoncrysol.2004.07.069

Figure 8

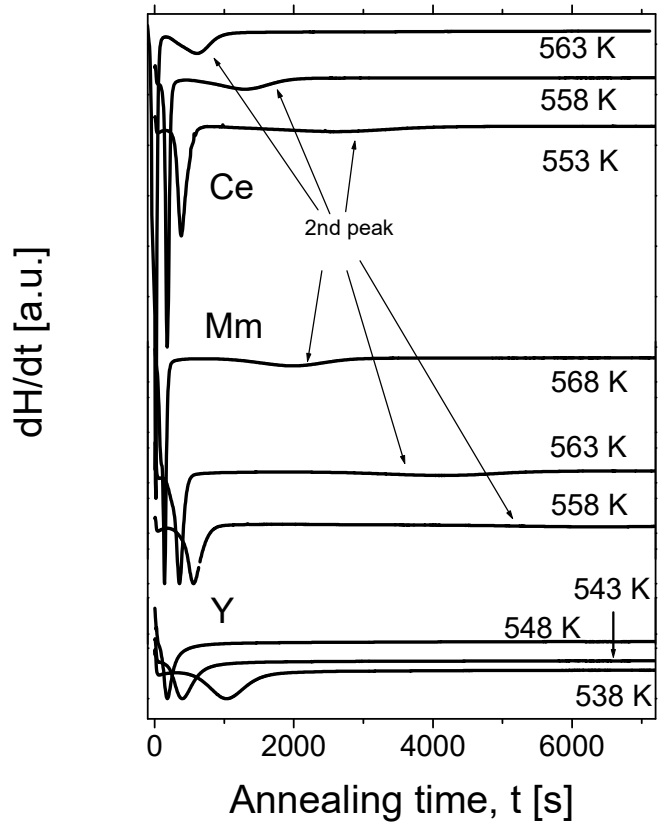

Journal of Non Crystalline Solids. Vol. 351. Núm. 2. 2005. Pag. 158-166
http://dx.doi.org/10.1016/j.jnoncrysol.2004.07.069

Figure 8BIS

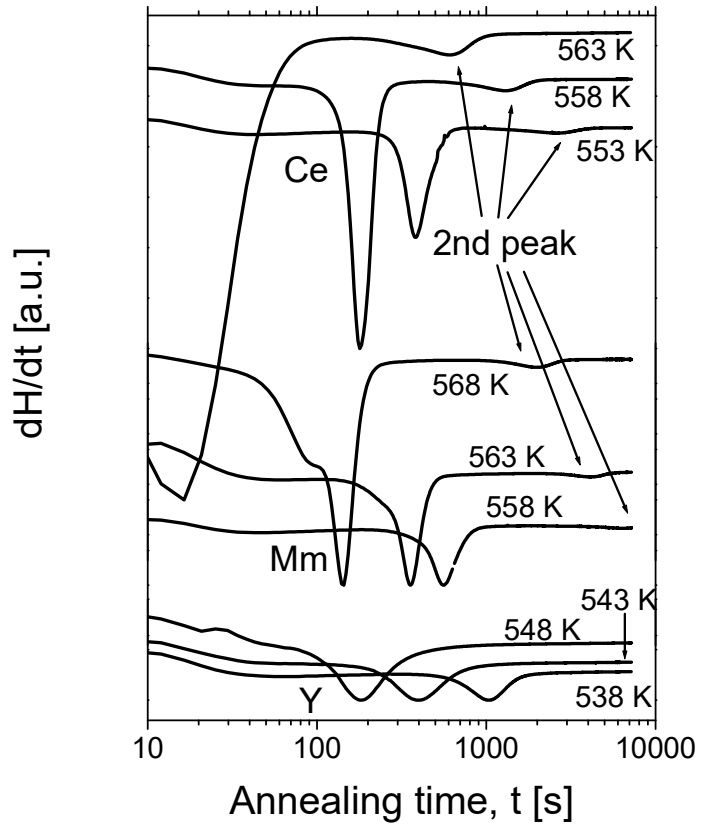

Journal of Non Crystalline Solids. Vol. 351. Núm. 2. 2005. Pag. 158-166
http://dx.doi.org/10.1016/j.jnoncrysol.2004.07.069

Figure 9

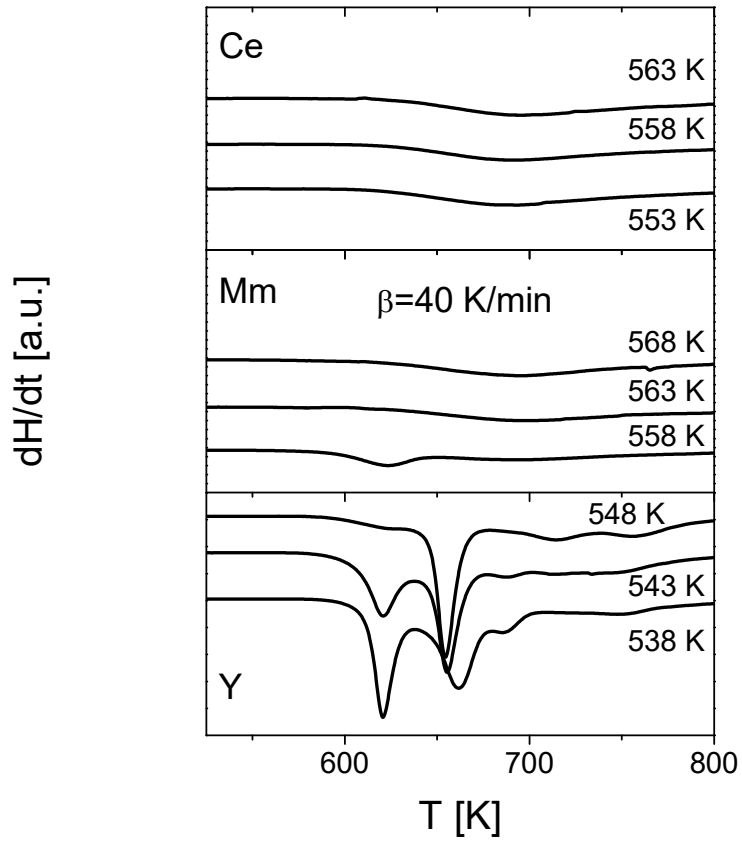

Journal of Non Crystalline Solids. Vol. 351. Núm. 2. 2005. Pag. 158-166
http://dx.doi.org/10.1016/j.jnoncrysol.2004.07.069

Figure 10

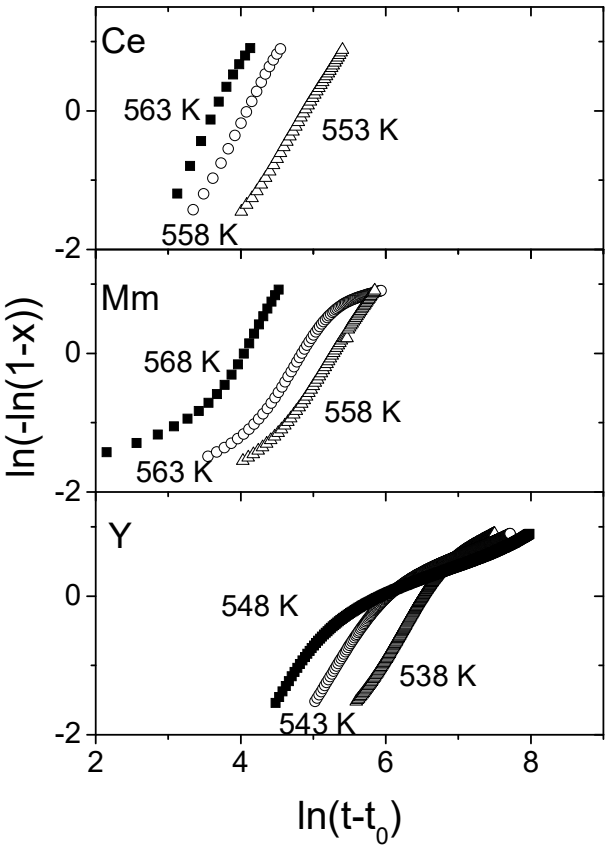

Figure 11

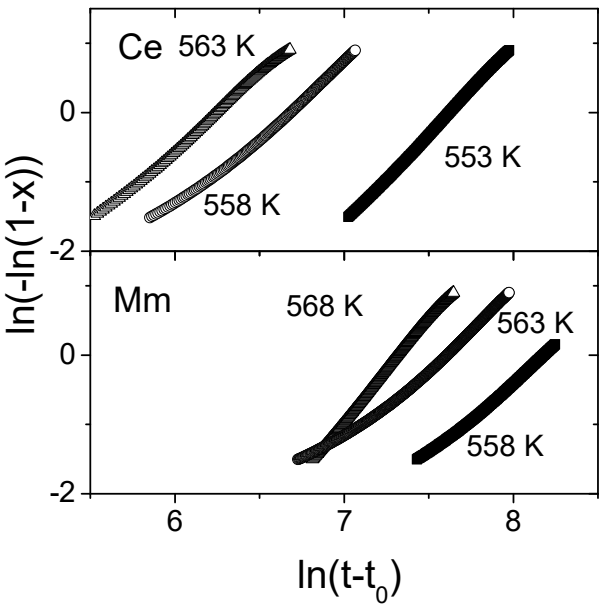

Journal of Non Crystalline Solids. Vol. 351. Núm. 2. 2005. Pag. 158-166
http://dx.doi.org/10.1016/j.jnoncrysol.2004.07.069

Figure 12